Eur. Phys. J. B **26**, 439–447 (2002)
DOI: 10.1140/epjb/e20020112

THE EUROPEAN PHYSICAL JOURNAL B
EDP Sciences

Classical spin liquid properties of the infinite-component spin vector model on a fully frustrated two dimensional lattice

B. Canals[1,a] and D.A. Garanin[2]

[1] Laboratoire Louis Néel, CNRS, 25 avenue des Martyrs, BP 166, 38042 Grenoble Cedex 9, France
[2] Max-Planck-Institut für Physik komplexer Systeme, Nöthnitzer Strasse 38, 01187 Dresden, Germany

Received 16 November 2001 and Received in final form 12 February 2002

Abstract. Thermodynamic quantities and correlation functions (CFs) of the classical antiferromagnet on the checkerboard lattice are studied for the exactly solvable infinite-component spin-vector model, $D \to \infty$. In contrast to conventional two-dimensional magnets with continuous symmetry showing extended short-range order at distances smaller than the correlation length, $r \lesssim \xi_c \propto \exp(T^*/T)$, correlations in the checkerboard-lattice model decay already at the scale of the lattice spacing due to the strong degeneracy of the ground state characterized by a macroscopic number of strongly fluctuating local degrees of freedom. At low temperatures, spin CFs decay as $\langle \mathbf{S}_0 \mathbf{S}_r \rangle \propto 1/r^2$ in the range $a_0 \ll r \ll \xi_c \propto T^{-1/2}$, where a_0 is the lattice spacing. Analytical results for the principal thermodynamic quantities in our model are very similar with MC simulations, exact and analytical results for the classical Heisenberg model ($D = 3$) on the pyrochlore lattice. This shows that the ground state of the infinite-component spin vector model on the checkerboard lattice is a classical spin liquid.

PACS. 75.10.Hk Classical spin models – 75.50.Ee Antiferromagnetics – 75.40.Cx Static properties (order parameter, static susceptibility, heat capacities, critical exponents, etc.)

1 Introduction

Frustrated magnets are particularly interesting as they often involve unusual low temperature magnetic behaviors. Depending on the nature of interactions, the local connectivity, spin dimensionality, these systems stabilize unconventional magnetic ground states such as non collinear Néel orders, topological spin glasses, classical or quantum spin liquids, spin ices [1]. These observations are both experimental and theoretical eventhough some of them, like topological spin glasses, are still conjectures. Among these ground states, two families have a striking property. Spin liquids, as well as spin ices, possess a residual entropy at zero temperature. This anomaly and the paradox it raises when considering the third principle of thermodynamics, are major points that people have tried to answer.

Theoretical studies of frustrated antiferromagnets started half a century ago with the exact solution of the triangular Ising antiferromagnet by Wannier [2]. In the following years, many lattices have been identified where spin models, from Ising symmetry (Z_2) to Heisenberg symmetry (O(3) or SU(2)), have disordered ground states. Among them, two have attracted a lot of interest: the kagomé lattice and the pyrochlore lattice [1]. The first one is a two dimensional arrangement of corner sharing triangles, while the latter is a three dimensional structure of corner sharing tetrahedra. When considering antiferromagnetic nearest neighbour interactions, they both display spin liquid like behaviors, well characterized theoretically. Spin-spin correlations functions are exponentially decaying at finite temperatures, even sometimes at $T = 0$, in both classical and quantum cases.

Recently, another lattice has received attention as it can be described as the two dimensional analog of the pyrochlore lattice: the checkerboard lattice. One very interesting point in this lattice is that its geometry mimics the local environment of each site of the pyrochlore lattice, but is much more simpler as it is two dimensional, and based on a square lattice structure. This has allowed Lieb and Schupp [3] to establish exact results in the quantum case ($S = 1/2$) showing that the spectrum in this system is very peculiar as ground states are necesseraly singlets in finite size clusters. For $S \geq 1$, it has been shown numerically [4] within an $1/S$ expansion that the ground state may have a local magnetization at zero temperature while for $S = 1/2$ it was proposed that the system orders in a valence bond solid ground state. A recent work [5] derived a phase diagram of the ground states for varying S stating that this system is most likely ordered for all S. Exact

[a] e-mail: canals@labs.polycnrs-gre.fr

diagonalization of finite clusters [6] for $S = 1/2$ reached the same conclusion and define the ground state as a 4-spin valence bond solid. A perturbative expansion also found a 4-spin valence bond solid [7] but with a different unit cell. There are now strong evidences that for small S this system should have long range order in a valence bond solid order parameter.

In this paper, we look for an exact solution on this lattice in the opposite limit of high spin dimensionality. Therefore, we study a classical Hamiltonian that corresponds to the generalisation of the Heisenberg model with D-component spin vectors [8,9]

$$\mathcal{H} = -\frac{1}{2}\sum_{rr'} J_{rr'}\mathbf{s}_r \cdot \mathbf{s}_{r'}, \qquad |\mathbf{s}_r| = 1 \tag{1}$$

and taking the limit $D \to \infty$. In this limit the problem becomes exactly solvable for all lattice dimensionalities, d, and the partition function of the system coincides [10] with that of the spherical model [11,12]. The $D = \infty$ model properly accounts for the profound role played, especially in low dimensions, by the Goldstone or would be Goldstone modes. At the same time, the less significant effects of the critical fluctuation coupling leading, *e.g.*, to the quantitatively different nonclassical critical indices, die out in the limit $D \to \infty$. Thus this model is a relatively simple yet a powerful tool for classical spin systems. It should not be mixed up with the N-flavour generalization of the quantum $S = 1/2$ model [13] in the limit $N \to \infty$, including its $1/N$ expansion [14,15]. The N-component nonlinear sigma model (see, *e.g.*, Refs. [16], as well as Refs. [17,18] for the $1/N$ expansion) is a quantum extension of equation (1) in the long-wavelength region at low temperatures. Effective free energies for the n-component order parameter appear, instead of equation (1), in conventional theories of critical phenomena. Using them for the $1/n$ expansion (see, *e.g.*, Ref. [19]) is a matter of taste. While yielding the same results for the critical indices as the lattice-based $1/D$ expansion [20–22], it misses the absolute values of the nonuniversal quantities.

In the following, we give the solution of this model on the checkerboard lattice and show that its ground state is a classical spin liquid. Particularly, it is shown that many properties are similar to the pyrochlore lattice case [23] despite the difference of lattice dimensionality. This strongly suggests that these frustrated systems are mainly driven by their local environment, *i.e.* by their topological frustration, at least for $D \to \infty$. The rest of this article is organized as follows. In Section 2 the structure of the checkerboard lattice and its collective spin variables are described. In Section 3 the formalism of the $D = \infty$ model is tailored for the checkerboard lattice. The diagrams of the classical spin diagram technique that do not disappear in the limit $D \to \infty$ are summed up. The general analytical expressions for the thermodynamic functions and spin CFs for all temperatures are obtained. In Section 4 the thermodynamic quantities of the checkerboard antiferromagnet are calculated and compared with MC simulation results as well as exact and analytical results previously obtained on the pyrochlore lattice in the whole temperature range. In Section 5 the real space correlation functions are computed. We finally discuss our results in Section 6 and conclude.

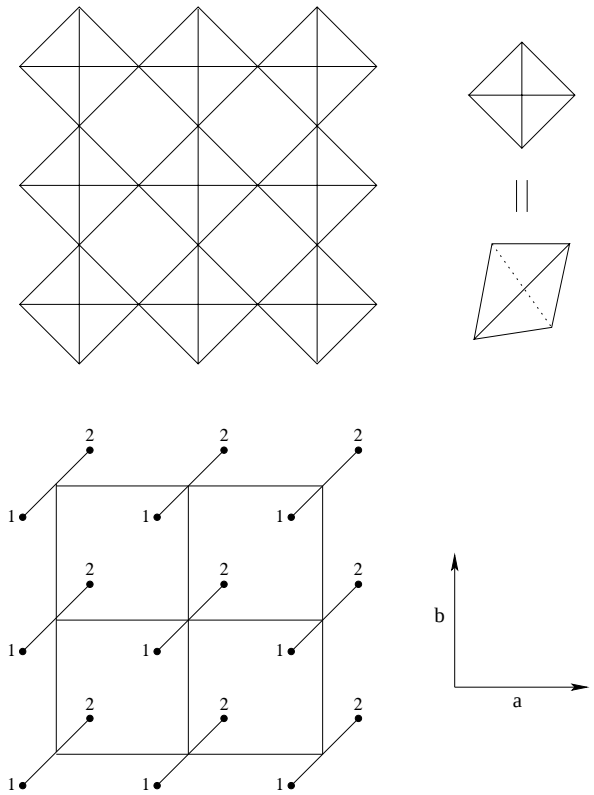

Fig. 1. The checkerboard lattice. It can be pictured as a square lattice of tetrahedra (top). Locally, it reproduces the same environment as the three dimensional pyrochlore lattice. In our calculations, it has been described by a square lattice with a 2-spins unit cell (bottom).

2 Lattice structure and the Hamiltonian

Checkerboard lattice shown in Figure 1 consists of corner-sharing tetrahedra. Each node of the corresponding Bravais lattice (*i.e.*, each elementary tetrahedron in Fig. 1) is numbered by $i, j = 1, \ldots, N$. Each site of the elementary tetrahedron is labeled by the index $l = 1, 2$. It is convenient to use the dimensionless units in which the interatomic distance equals $1/2$ and hence the lattice period equals 1. The tetrahedra numbered by $i, j = 1, \ldots, N$ can be obtained from each other by the translations

$$\mathbf{r}_j^l = \mathbf{r}_i^l + n_u\mathbf{u} + n_v\mathbf{v}, \tag{2}$$

where $\mathbf{r}_i^l$ is the position of a site on the lattice, n_u and n_v are integers, $\mathbf{u}$ and $\mathbf{v}$ are the elementary translation vectors (lattice periods), and

$$\mathbf{u} = (1, 0), \qquad \mathbf{v} = (0, 1). \tag{3}$$

To facilitate the diagram summation in the next section, it is convenient to put the Hamiltonian (1) into a

diagonal form. First, one goes to the Fourier representation according to

$$\mathbf{s}^l_{\mathbf{q}} = \sum_i \mathbf{s}^l_i \mathrm{e}^{-\mathrm{i}\mathbf{q}\cdot\mathrm{r}^l_i}, \qquad \mathbf{s}^l_i = \frac{1}{N}\sum_{\mathbf{q}} \mathbf{s}^l_{\mathbf{q}} \mathrm{e}^{\mathrm{i}\mathbf{q}\cdot\mathrm{r}^l_i}, \tag{4}$$

where the wave vector $\mathbf{q}$ belongs to the square Brillouin zone $\mathrm{Bz}_{\mathrm{kx,ky}} = [-\pi,\pi]\times[-\pi,\pi]$ (see Fig. 1). The Fourier-transformed Hamiltonian reads

$$\mathcal{H} = \frac{1}{2N}\sum_{ll'\mathbf{q}} V^{ll'}_{\mathbf{q}}\, \mathbf{s}^l_{\mathbf{q}}\cdot \mathrm{s}^{l'}_{-\mathbf{q}}, \tag{5}$$

where the interaction matrix is given by

$$\hat{V}_{\mathbf{q}} = 2J \begin{pmatrix} a & 2uv \\ 2uv & b \end{pmatrix} \tag{6}$$

with $a = \cos(q_x)$, $b = \cos(q_y)$, $u = \cos(q_x/2)$ and $v = \cos(q_y/2)$.

At the second stage, the Hamiltonian (5) is finally diagonalized to the form

$$\mathcal{H} = \frac{1}{2N}\sum_{n\mathbf{q}} \tilde{V}^n_{\mathbf{q}}\, \sigma^n_{\mathbf{q}}\cdot\sigma^n_{-\mathbf{q}}, \tag{7}$$

where $\tilde{V}^n_{\mathbf{q}} = 2J\nu_n(\mathbf{q})$ are the eigenvalues of the matrix $V^{ll'}_{\mathbf{q}}$ taken with the negative sign,

$$\nu_1 = 1, \qquad \nu_2 = -(1+\cos(q_x)+\cos(q_y)). \tag{8}$$

The diagonalizing transformation has the explicit form

$$U^{-1}_{nl}(\mathbf{q}) V^{ll'}_{\mathbf{q}} U_{l'n'}(\mathbf{q}) = \tilde{V}^n_{\mathbf{q}}\delta_{nn'}, \tag{9}$$

where the summation over the repeated indices is implied and $\hat{U}$ is the real unitary matrix, $\hat{U}^{-1} = \hat{U}^T$, *i.e.*, $U^{-1}_{nl} = U_{ln}$. The columns of the matrix $\hat{U}$ are the two normalized eigenvectors $U_n = (U_{1n}, U_{2n})$ of the interaction matrix $\hat{V}$:

$$U_1 = \sqrt{\frac{1+a}{2+a+b}}\left(-\frac{2uv}{1+a}, 1\right),$$
$$U_2 = \sqrt{\frac{1+b}{2+a+b}}\left(\frac{1+a}{2uv}, 1\right). \tag{10}$$

The normalized eigenvectors satisfy the requirements of orthogonality and completeness, respectively:

$$U_{ln}(\mathbf{q})U_{ln'}(\mathbf{q}) = \delta_{nn'}, \qquad U_{ln}(\mathbf{q})U_{l'n}(\mathbf{q}) = \delta_{ll'}. \tag{11}$$

The Fourier components of the spins $\mathbf{s}^l_{\mathbf{q}}$ and the collective spin variables $\sigma^n_{\mathbf{q}}$ are related by

$$\mathbf{s}^l_{\mathbf{q}} = U_{ln}(\mathbf{q})\sigma^n_{\mathbf{q}}, \qquad \sigma^n_{\mathbf{q}} = \mathbf{s}^l_{\mathbf{q}} U_{ln}(\mathbf{q}). \tag{12}$$

The largest dispersionless eigenvalue ν_1 of the interaction matrix (see Eq. (8)) manifests frustration in the system which precludes an extended short-range order even in the limit $T \to 0$. Independence of ν_1 of $\mathbf{q}$ signals that

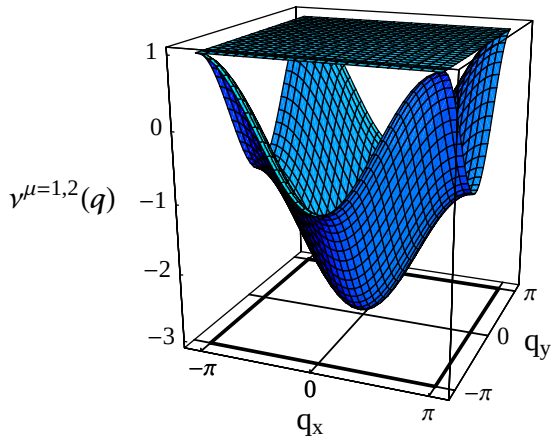

Fig. 2. Reduced eigenvalues of the interaction matrix, $\nu_n(\mathbf{q}) = \tilde{V}^n_{\mathbf{q}}/(2J)$ of equation (7), plotted over the Brillouin zone. The flat band signals that half of the degrees of freedom in this system can rotate freely.

1/2 of all spin degrees of freedom are local and can rotate freely. The other eigenvalue satisfy

$$\nu_2(\mathbf{q}) \cong -3 + q^2/2 \tag{13}$$

at small wave vectors, $q^2 \equiv q_x^2 + q_y^2 \ll 1$. Within our description of the checkerboard lattice, the would be usual Goldstone mode corresponds to ν_2. At the corners of the Brillouin zone $(\pm\pi, \pm\pi)$, this mode becomes degenerate with the flat one and defines low energy excitations.

$$\nu_2(\tilde{\mathbf{q}}) \cong 1 - \tilde{q}^2/2 \tag{14}$$

where $q = (\pm\pi, \pm\pi) + \tilde{q}$, $|\tilde{q}| \ll 1$. It is the equivalent of the usual Goldstone mode that is present in low-dimensional magnets with a continuous symmetry. Thus, it is this mode that will be associated with a correlation length, as we will see in Section 5. It is remarkable that this mode contains all information about dispersive excitations present in this model. If we had choosen a four sites unit cell [24] instead of a two sites one, we would have obtained a similar description as the one done on the pyrochlore antiferromagnet [23]. Then, an "optical" mode would have been recovered, *i.e.* a mode with a finite energy gap for all wave vector; the usual Goldstone mode would have been degenerate with the flat one at $q = 0$ and the lowest not dispersive branch, would have been two times degenerate. This clearly shows the similarity of these two lattices as it is expected because of the exact equivalence of the local environment of each site. The $\mathbf{q}$ dependences of the eigenvalues ν_n over the whole Brillouin zone are shown in Figure 2.

In the next section the equations describing spin correlation functions of the classical checkerboard antiferromagnet in the large-D limit will be obtained with the help of the classical spin diagram technique. The readers who are not interested in details can skip to equation (16) or directly to Section 4.

3 Classical spin diagram technique and the large-D limit

The exact equations for spin correlation functions in the limit $D \to \infty$, as well as the $1/D$ corrections, can be the most conveniently obtained with the help of the classical spin diagram technique [25–27]. A complete description of the technique applied to a non bipartite lattice can be found in reference [28]. We only give here an outline of the calculations.

Our goal is to compute spin-spin CF's

$$s^{ll'}(\mathbf{q}) = \langle s^n_{\mathbf{q}} s^n_{-\mathbf{q}} \rangle \tag{15}$$

which are related to CF's of the σ variables

$$\sigma^n(\mathbf{q}) = \frac{D}{N}\langle \sigma^n_{\alpha\mathbf{q}} \sigma^n_{\alpha,-\mathbf{q}} \rangle = \frac{1}{N}\langle \sigma^n_{\mathbf{q}} \sigma^n_{-\mathbf{q}} \rangle, \tag{16}$$

through the relation

$$s^{ll'}(\mathbf{q}) = U_{ln}(\mathbf{q}) U_{l'n}(\mathbf{q}) \sigma^n(\mathbf{q}) \tag{17}$$

following from equation (12).

The analytical expression for the σ CF in the SCGA has the Ornstein-Zernike form

$$\sigma^n(\mathbf{q}) = \frac{D\tilde{\Lambda}}{1 - \tilde{\Lambda}\beta\tilde{V}^n_{\mathbf{q}}} \cdot \tag{18}$$

In the large-D limit the expression of $\tilde{\Lambda}$ simplifies [25] and is given by

$$\tilde{\Lambda} = \frac{2}{D} \frac{1}{1 + \sqrt{1 + 8L/D}} \cdot \tag{19}$$

Here the dispersion L is given by the formula

$$L = \frac{\tilde{\Lambda}}{2 \cdot 2!} \sum_n v_0 \int \frac{\mathrm{d}\mathbf{q}}{(2\pi)^d} \frac{(\beta\tilde{V}^n_{\mathbf{q}})^2}{1 - \tilde{\Lambda}\beta\tilde{V}^n_{\mathbf{q}}} \cdot \tag{20}$$

The summation $(1/N)\sum_{\mathbf{q}} \ldots$ is replaced by the integration over the Brillouin zone, v_0 is the unit cell volume, and d is the spatial dimensionality. For the square lattice we have $v_0 = 1$. The expression for L can be simplified to

$$L = \frac{\bar{P} - 1}{2\tilde{\Lambda}}, \qquad \bar{P} \equiv \frac{1}{2}\sum_n P_n, \tag{21}$$

where P_n is the lattice Green function associated with the eigenvalue n:

$$P_n = v_0 \int \frac{\mathrm{d}\mathbf{q}}{(2\pi)^d} \frac{1}{1 - \tilde{\Lambda}\beta\tilde{V}^n_{\mathbf{q}}} \cdot \tag{22}$$

Now one can eliminate L from equations (19, 21), which yields the basic equation of the large-D model,

$$D\tilde{\Lambda}\bar{P} = 1. \tag{23}$$

This nonlinear equation determining $\tilde{\Lambda}$ as a function of temperature differs from those considered earlier [25–27,29] by a more complicated form of $\bar{P}$ reflecting the lattice structure. The form of this equation is similar to that appearing in the theory of the usual spherical model [11,12]. The meanings of both equations are, however, different. Whereas in the standard spherical model a similar equation account for the pretty unphysical global spin constraint, equation (23) here is, in fact, the normalization condition $\langle \mathbf{s}^2_{\mathbf{r}} \rangle = 1$ for the spin vectors on each of the lattice sites $\mathbf{r}$. Indeed, calculating the spin autocorrelation function in the form symmetrized over sublattices with the help of equations (17, 11), and (18), one obtains

$$\begin{aligned} \langle \mathbf{s}^2_{\mathbf{r}} \rangle &= v_0 \int \frac{\mathrm{d}\mathbf{q}}{(2\pi)^d} \frac{1}{2} \sum_l s^{ll}(\mathbf{q}) \\ &= v_0 \int \frac{\mathrm{d}\mathbf{q}}{(2\pi)^d} \frac{1}{2} \sum_n \sigma^n(\mathbf{q}) = D\tilde{\Lambda}\bar{P}. \end{aligned} \tag{24}$$

That is, the spin-normalization condition is automatically satisfied in our theory by virtue of equation (23). After $\tilde{\Lambda}$ has been found from this equation, the spin CFs are readily given by equations (18, 17).

To avoid possible confusions, we should mention that in the paper of Reimers, reference [30], where equation (18) with the bare cumulant $\Lambda = 1/D$ has been obtained, the theoretical approach has been called "Gaussian approximation (GA)". This term taken from the conventional theory of phase transitions based on the Landau free-energy functional implies that the Gaussian fluctuations of the *order parameter* are considered. In the microscopic language, this merely means calculating correlation functions of fluctuating spins after applying the MFA. Such an approach is known to be inconsistent, since correlations are taken into account after they had been neglected. As a result, for the checkerboard lattice one obtains a phase transition at the temperature $T_c = T_c^{\mathrm{MFA}} = 2J/D$ but immediately finds that the approach breaks down below T_c because of the infinitely strong fluctuations. In contrast to this MFA-based approach, the self-consistent Gaussian approximation used here allows, additionally, to the Gaussian fluctuations of the *molecular field*, which renormalize $\tilde{\Lambda}$ and lead to the absence of a phase transition for this class of systems. The SCGA is, in a sense, a "double-Gaussian" approximation; one concerning fluctuations of the order parameter and the other one describing fluctuations of the molecular field.

To close this section, let us work out the expressions for the energy and the susceptibility of the checkerboard antiferromagnet. For the energy of the whole system, using equations (7, 16), as well as the equivalence of all spin components, one obtains

$$U_{\mathrm{tot}} = \langle \mathcal{H} \rangle = -\frac{N}{2} \sum_n v_0 \int \frac{\mathrm{d}\mathbf{q}}{(2\pi)^d} \tilde{V}^n_{\mathbf{q}} \sigma^n(\mathbf{q}). \tag{25}$$

To obtain the energy pro spin U, one should divide this expression by $2N$. With the use of equation (18), the latter

can be expressed through the lattice Green's function $\bar{P}$ of equation (21); then with the help of equation (23) it can be put into the final form

$$U = \frac{T}{2}\left(D - \frac{1}{\tilde{\Lambda}}\right). \tag{26}$$

The susceptibility pro spin symmetrized over sublattices can be expressed through the spin CFs as

$$\chi_{\mathbf{q}} = \frac{1}{2DT}\sum_{ll'} s^{ll'}(\mathbf{q}). \tag{27}$$

With the use of equation (17) this can be rewritten in the form

$$\chi_{\mathbf{q}} = \frac{1}{2DT}\sum_{n} W_n^2(\mathbf{q})\sigma^n(\mathbf{q}), \qquad W_n(\mathbf{q}) \equiv \sum_{l} U_{ln}(\mathbf{q}), \tag{28}$$

where the diagonalized CFs are given by equation (18). From equation (10) it follows that in the limit $\mathbf{q} \to 0$ one has $W_1 = 0$ and $W_2 = \sqrt{2}$. Thus the homogeneous susceptibility $\chi \equiv \chi_0$ simplifies to

$$\chi = \frac{1}{DT}\sigma^2(0). \tag{29}$$

As we shall see in the next section, disappearance of the terms with $n = 1$ from this formula ensures the nondivergence of the homogeneous susceptibility of the checkerboard antiferromagnet in the limit $T \to 0$. The situation for $\mathbf{q} \neq 0$ is much more intricate and it will be considered below in relation to the neutron scattering cross section.

4 Thermodynamics of the checkerboard antiferromagnet

To put the results obtained above into the form explicitly well behaved in the large-D limit and allowing a direct comparison with the results obtained by other methods for systems with finite values of D, it is convenient to use the mean-field transition temperature $T_c^{\mathrm{MFA}} = 2J/D$ as the energy scale. With this choice, one can introduce the reduced temperature θ and the so-called gap parameter G according to

$$\theta \equiv \frac{T}{T_c^{\mathrm{MFA}}}, \qquad G \equiv \frac{D}{\theta}\tilde{\Lambda}. \tag{30}$$

In these terms, equation (23) rewrites as

$$\theta G \bar{P}(G) = 1 \tag{31}$$

and determines G as function of θ. Here $\bar{P}(G)$ is defined by equation (21), where

$$P_1 = \frac{1}{1-G}, \qquad P_2 = v_0 \int \frac{\mathrm{d}\mathbf{q}}{(2\pi)^d}\frac{1}{1 - G\nu_2(\mathbf{q})}, \tag{32}$$

The σ CFs of equation (18), which are proportional to the integrands of P_n, can be rewritten in the form

$$\sigma^n(\mathbf{q}) = \frac{\theta G}{1 - G\nu_n(\mathbf{q})}\,. \tag{33}$$

Further, it is convenient to consider the reduced energy pro spin defined by

$$\tilde{U} \equiv U/|U_0|, \qquad U_0 = -J, \tag{34}$$

where U_0 is the energy pro spin at zero temperature. With the help of equation (26) $\tilde{U}$ can be written as

$$\tilde{U} = \theta - 1/G. \tag{35}$$

The homogeneous susceptibility χ of equation (29) can be rewritten with the help of equation (13) in the reduced form

$$\tilde{\chi} \equiv 2J\chi = \frac{G}{1+3G}\,. \tag{36}$$

The sense of calling G the "gap parameter" is clear from equation (33). If $G = 1$, then the gap in correlation functions closes: σ^1 turns to infinity, and σ^2 diverges at $q \to (\pm\pi, \pm\pi)$. For nonordering models, it happens only in the limit $\theta \to 0$, however. The solution of equation (31) satisfies $G \leq 1$ and goes to zero at high temperatures. If $\theta \ll 1$, the function $\bar{P}$ is dominated by $P_1 = 1/(1-G)$. The ensuing asymptotic form of the gap parameter at low temperatures reads

$$G \cong 1 - \frac{\theta}{2}, \qquad \theta \ll 1. \tag{37}$$

At high temperatures, equation (31) requires small values of G. Here, the limiting form of $\bar{P}$ can be shown to be $\bar{P} \cong 1 + (3/2)G^2$. The corresponding asymptote of G has the form

$$G \cong \frac{1}{\theta}\left(1 - \frac{3}{2\theta^2}\right), \qquad \theta \gg 1. \tag{38}$$

The numerically calculated temperature dependence of G is shown in Figure 3. Note that in the MFA one has $G = 1/\theta$ which attains the value 1 at $\theta = 1$.

The temperature dependence of the reduced energy of equation (35) is shown in Figure 4. Its asymptotic forms following from equations (37, 38) are given by

$$\tilde{U} \cong \begin{cases} -3/(2\theta), & \theta \gg 1 \\ -1 + \theta/2, & \theta \ll 1. \end{cases} \tag{39}$$

This implies the reduced heat capacity $\tilde{C} = \mathrm{d}\tilde{U}/\mathrm{d}\theta$ equal to $1/2$ at low temperatures. To compare with the MC simulation data of reference [31] for the heat capacity of the Heisenberg model we will use, instead of $\tilde{C}$, the true heat capacity $C = dU/dT = (D/2)\tilde{C}$ (see Eqs. (30, 34)), which in our approach tends to $D/4 \Rightarrow 3/4$ at low temperatures.

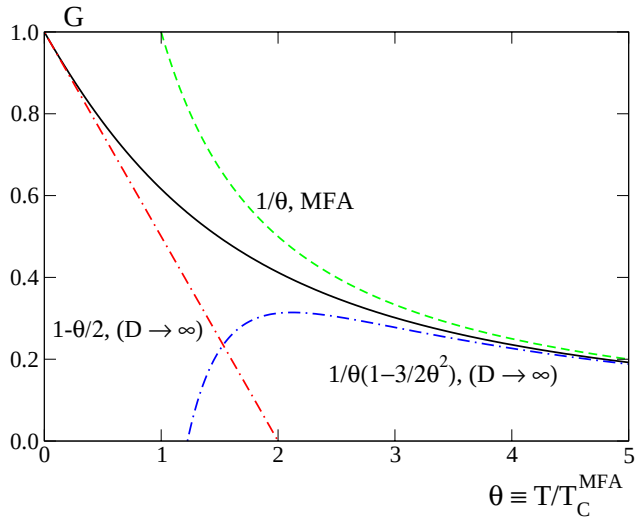

Fig. 3. Temperature dependence of the gap parameter G for the checkerboard antiferromagnet.

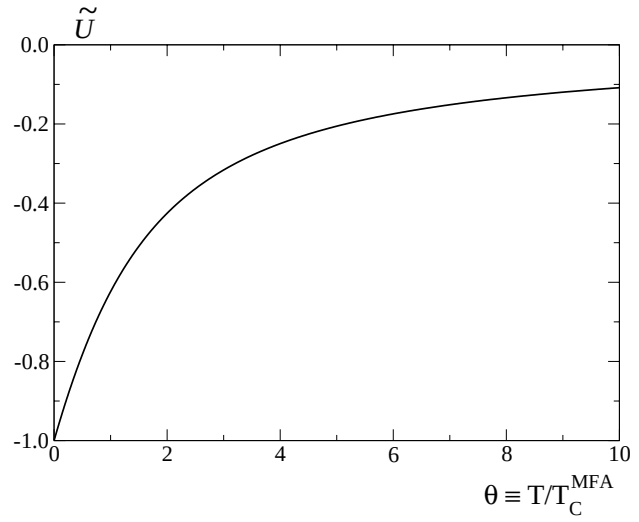

Fig. 4. Temperature dependence of the reduced energy for the checkerboard antiferromagnet.

The temperature dependence of the heat capacity, compared with previous MC results of the Heisenberg antiferromagnet on the pyrochlore lattice [31] as well as exact solution of the infinite component classical antiferromagnet on the pyrochlore lattice [23] are shown in Figure 5. We see that the behavior of these two different models [31,23] on the pyrochlore lattice are very similar to our results on the checkerboard lattice, thus confirming the analogy of these two structures despite their different space dimensionality.

Using equation (39) we compute the low and high temperature asymptotic behavior of the reduced susceptibility $\tilde{\chi}$

$$\tilde{\chi} \cong \begin{cases} 1/4 - \theta/32, & \theta \ll 1 \\ (1/\theta)(1 - 3/\theta), & \theta \gg 1. \end{cases} \quad (40)$$

Its dependence at all temperatures is reported in Figure 6. Here also, we recover a behavior very similar to the one

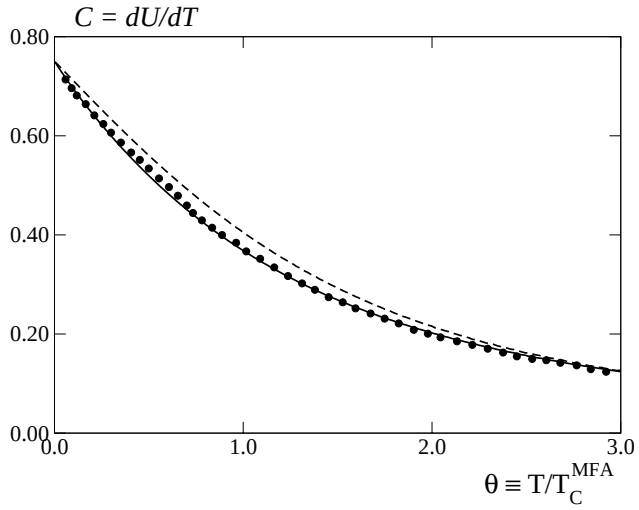

Fig. 5. Temperature dependence of the heat capacity of the checkerboard antiferromagnet. The MC results of reference [31] for the Heisenberg model ($D = 3$) on the pyrochlore lattice are represented by circles. Black line corresponds to the exact solution of the infinite component Heisenberg antiferromagnet on the pyrochlore lattice [23]. Dashed line corresponds to the exact solution of the infinite component Heisenberg antiferromagnet on the checkerboard lattice.

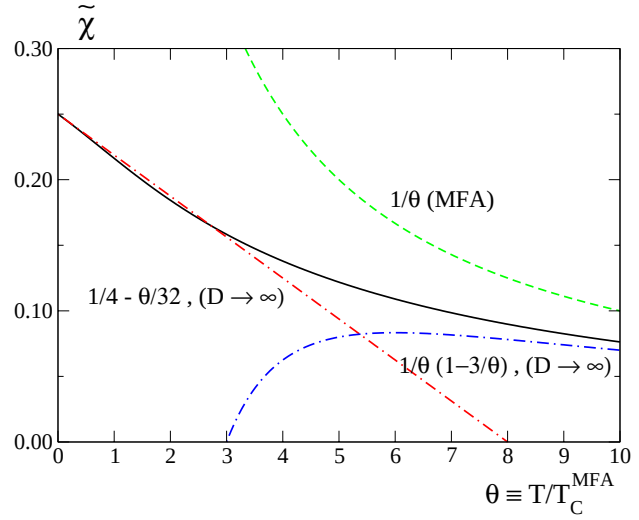

Fig. 6. Temperature dependence of the reduced uniform susceptibility of the checkerboard antiferromagnet. Asymptotes for high and low temperatures are given, for both the infinite component model and the mean field case.

of the pyrochlore lattice where MC simulations and analytical results have been obtained for the Heisenberg antiferromagnet [32] as well as exact results for the infinite component classical antiferromagnet [23]. The similarity between our results and the local approximation [33] developed in reference [32] suggest that the checkerboard antiferromagnet has its thermodynamics governed by local correlations, as it is expected in a classical spin liquid.

5 Real-space correlation functions

The low-temperature behavior of the σ correlation functions of equation (33) is dominated by their asymptotic form at small wave vectors, where the would be Goldstone mode is defined, *i.e.* at $q = (\pm\pi, \pm\pi) + \tilde{q}$, $|\tilde{q}| \ll 1$. According to equations (8), we find, (14), and (37), by

$$\sigma^1 \cong 2, \qquad \sigma^2 \cong \frac{2\kappa^2}{\kappa^2 + \tilde{q}^2} \tag{41}$$

where the quantity $\kappa^2 = \theta$ in σ^2 defines the correlation length

$$\xi_c = \frac{1}{\kappa} = \frac{1}{\sqrt{\theta}} \cdot \tag{42}$$

Appearance of this length parameter implies that the real-space spin CFs defined, according to equations (17, 4), by

$$s_{ij}^{ll'} = v_0 \int \frac{\mathrm{d}\mathbf{q}}{(2\pi)^d} \mathrm{e}^{\mathrm{i}\mathbf{q}\cdot(\mathbf{r}_i^l - \mathbf{r}_j^{l'})} U_{ln}(\mathbf{q}) U_{l'n}(\mathbf{q}) \sigma^n(\mathbf{q}) \tag{43}$$

decay exponentially at large distances at nonzero temperatures. In contrast to conventional lattices, divergence of ξ_c at $\theta \to 0$ does not lead here to an extended short-range order, *i.e.*, to strong correlation at distances $r \lesssim \xi_c$. The zero-temperature CFs are *purely geometrical* quantities which are dominated by σ^1 and have the form

$$s_{ij}^{ll'} = 2v_0 \int \frac{\mathrm{d}\mathbf{q}}{(2\pi)^d} \mathrm{e}^{\mathrm{i}\mathbf{q}\cdot(\mathbf{r}_i^l - \mathbf{r}_j^{l'})} U_{l1}(\mathbf{q}) U_{l'1}(\mathbf{q}). \tag{44}$$

It is convenient to enumerate CFs by the numbers n_u and n_v defined by equation (2). Thus $s_{n_u,n_v}^{ll'}$ is the correlation function of the l sublattice spin of the "central" unit-cell $(0,0)$ with the l' sublattice spin of the unit-cell translated by (n_u, n_v). Let us calculate the CFs with $l = l' = 1$ at large distances along the horizontal line in Figure 1, at small but non zero temperature. We use the asymptotic form of the matrix $U_{ln}(\mathbf{q})$ for $q = (\pm\pi, \pm\pi) + \tilde{q}$, $|\tilde{q}| \ll 1$, as well as the asymptotic form of CFs in equation (41). This allows to write this correlation function as

$$\begin{aligned} s_{ij}^{ll'} &= v_0 \int \frac{\mathrm{d}\tilde{\mathbf{q}}}{(2\pi)^d} (-1)^n \mathrm{e}^{\mathrm{i}n\tilde{q}_x} \left(U_{11}^2(\tilde{\mathbf{q}}) \sigma^1 + U_{12}^2(\tilde{\mathbf{q}}) \sigma^2 \right) \\ &= 2v_0 \int \frac{\mathrm{d}\tilde{\mathbf{q}}}{(2\pi)^d} (-1)^n \mathrm{e}^{\mathrm{i}n\tilde{q}_x} \left(\frac{\tilde{q}_y^2}{\tilde{q}^2} + \frac{\tilde{q}_x^2}{\tilde{q}^2} \frac{\kappa^2}{\kappa^2 + \tilde{q}^2} \right) \cdot \end{aligned} \tag{45}$$

Simplifying this expression and taking into account that the integral of the cosine over the whole Brillouin zone is zero, one arrives at the asymptotic form

$$s_{n,0}^{11} \cong \frac{(-1)^n \kappa}{\pi n} K_1(\kappa n) \cong \begin{cases} \dfrac{(-1)^n}{\pi n^2}, & \kappa n \ll 1 \\ \dfrac{(-1)^n \kappa^2}{\sqrt{2\pi}} \dfrac{\mathrm{e}^{-\kappa n}}{(\kappa n)^{3/2}}, & \kappa n \gg 1, \end{cases} \tag{46}$$

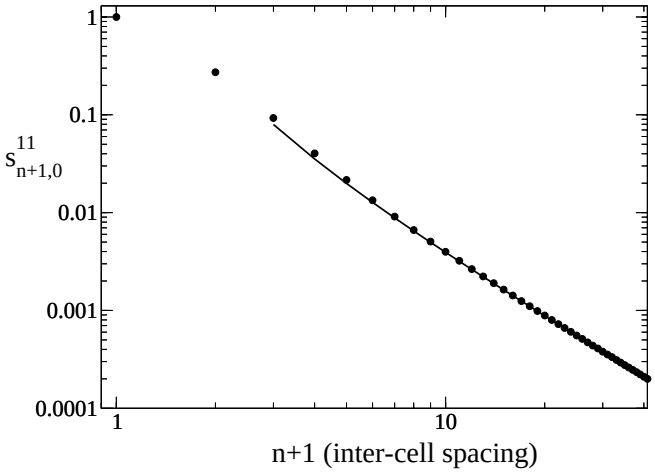

Fig. 7. Real-space correlation functions $s_{n,0}^{11}$ at $T = 0$ calculated from equation (44) along an horizontal line. The distance unit is the interatomic spacing. The asymptote given by equation (46) is shown by the dashed lines.

where $K_\nu(x)$ is the Macdonald (modified Bessel) function. The strong decrease of this correlation function with distance even at $T = 0$ ($\kappa = 0$) is not surprising, since our solution spans the whole highly degenerate ground-state manifold and this degeneracy is not lifted in the limit $D \to \infty$. At small but non zero temperature, spin-spin correlations are exponentially decaying as if interactions were renormalized to zero and drive this system to a paramagnetic fix point for finite temperatures. Let us calculate more generally the CFs with $l = 1, 2$ and $l' = 1, 2$ at large distances along the horizontal line in Figure 1, at zero temperature. Following the same previous procedure, we obtain

$$s_{n,0}^{11} = s_{n,0}^{22} = \frac{(-1)^n}{\pi n^2}, \qquad s_{n,0}^{12} = \frac{(-1)^n}{\pi (n + 1/2)^2} \tag{47}$$

where n is in unit of the inter-cell distance. We note that despite the divergence of the correlation length ξ_c when lowering the temperature, the model do not order, which clearly defines this system as a classical two dimensional spin liquid.

6 Discussion

In the main part of this article, we have presented in detail the exact solution for the $D = \infty$ component classical antiferromagnet on the checkerboard lattice. The solution does not show ordering at any temperature due to the strong degeneracy of the ground state, and thermodynamic functions behave smoothly. In contrast to conventional two-dimensional magnets, there is no extended short-range order at low temperature, and $T = 0$ is not a critical point of the system. Although the correlation associated to the would be Goldstone mode diverges as $\xi_c \propto T^{-1/2}$, the power law decay $\langle s_0 s_r \rangle \propto 1/r^2$ at zero temperature of the spin correlation functions leads to the

loss of correlations at the scale of the interatomic distance. All these properties characterize this model as a two-dimensional classical spin liquid. As these results are obtained within the $D = \infty$ component classical antiferromagnet, it is expected that it mimics the large S value Heisenberg antiferromagnet on the checkerboard lattice. Surprisingly, there are results [4,5] suggesting that for large S, the Heisenberg antiferromagnet should be ordered on this lattice. At this stage, the discrepancy between the different approaches is not clear. A possible explanation, as reported in reference [4], "is that for large S, there should be quantum order by disorder (as supported in [5]) but this order by disorder comes with an energy scale of J/S rather than J. Therefore, in the classical limit, the temperature at which the correlation length grows exponentially goes to zero. In other words, the limits $T \to 0$ and $S \to \infty$ (or $D \to \infty$) should not commute." Nevertheless, it should be stressed that even if there is a discrepancy at $T = 0$, for finite T, we expect the $D = \infty$ case to correctly describe the checkerboard Heisenberg antiferromagnet as any critical behavior is expected to appear only in the zero temperature neighbourhood. A similar problem has been encountered within the present formalism applied to kagomé antiferromagnet [28]. Here again, finite temperature properties of the infinite component spin vector model have been found to be close to the $D = 3$ Heisenberg case. However at $T \to 0$, the method misses the "order by disorder" phenomenon which selects the coplanar spin manifold. As a consequence, the $D = 3$ zero temperature specific heat is much closer to 1, $C = 11/12k_{\rm B}$, than it would be if really one third of the degrees of freedom were still fluctuating (as suggested by a mean field analysis). Whether $1/D$ corrections could resolve this discrepancy is still a work to be done.

Despite the dimensionality of the checkerboard lattice ($d = 2$), there are many similarities with previously obtained results on the pyrochlore lattice ($d = 3$). The specific heat has in particular, the same value at zero temperature [23,31] for $D = 3$. Susceptibility is also very similar with the one of the Heisenberg antiferromagnet as well as the infinite component classical antiferromagnet on the pyrochlore lattice. MC results, as well as exact and analytical results are very close to the one obtained here [23,32]. This is not surprising as the spin liquid behavior implies that the lattice is mainly described by local fluctuations. In fact, it is true at least for finite temperature thermodynamics. Why the present approach can lead to correct results for the pyrochlore case and not for the checkerboard case at very low temperatures has not been addressed in the present work. We can only note that the common point between the two lattices is the local connectivity which is clearly well taken into account within the $D \to \infty$ formalism. Whether dimensionality is relevant is not clear. At this stage, it can be noted that for the kagomé case, the $D \to \infty$ formalism has missed the reduced specific heat mechanism (see Refs. [28,34]) while for the pyrochlore case, it has been reproduced (see Ref. [23]) Therefore, discrepancies with $D = 3$ descriptions could be ascribed to dimensionality although other subtle phenomena that are not taken into account when $D \to \infty$ cannot be ruled out without studying the same model when including $1/D$ corrections.

To conclude, this classical approach indicates that for infinite component spin value, the checkerboard antiferromagnet should be disordered and behave as a spin liquid. We give some arguments why the present approach is at variance with results of reference [5]. It is interesting to note that for small spin value, the checkerboard antiferromagnet is expected to order [4–6]. Therefore the checkerboard antiferromagnet cannot be compared to the pyrochlore antiferromagnet even if its geometry defines it as its two dimensional analog. Even if they have the same unit cell, it is probably the global geometry of the underlying Bravais lattice that drives the physics and not only the local connectivity.

References

1. For a collection of articles, see *Magnetic systems with Competing Interactions: Frustated Spin System*, edited by H.T. Diep (World Scientific, Singapore, 1994); for Ising systems, see R. Liebmann, *Statistical Mechanics of Periodic Frustrated Ising Systems* (Springer, Berlin, 1986); for reviews, see A.P. Ramirez, Annu. Rev. Mater. Sci. **24**, 453 (1994); P. Schiffer, A.P. Ramirez, Comments Cond. Mat. Phys. **18**, 21 (1996); M.J. Harris, M.P. Zinkin, Mod. Phys. Lett. B **10**, 417 (1996).
2. G.H. Wannier, Phys. Rev. **79**, 357 (1950).
3. E.H. Lieb, P. Schupp, Phys. Rev. Lett. **83**, 5362 (1999).
4. B. Canals, to be published in Phys. Rev. B.
5. R. Moessner, O. Tchernyshyov, S.L. Sondhi, `cond-mat/0106286`.
6. J.-B. Fouet, M. Mambrini, P. Sindzingre, C. Lhuillier, to be published in Phys. Rev. B.
7. M. Elhajal, B. Canals, C. Lacroix, Can. J. Phys. **79**, 1353 (2001).
8. H.E. Stanley, Phys. Rev. Lett. **20**, 589 (1968).
9. H.E. Stanley, in *Phase Transitions and Critical Phenomena*, edited by C. Domb, M.S. Green (Academic Press, New York, 1974), Vol. 3.
10. H.E. Stanley, Phys. Rev. **176**, 718 (1968).
11. T.N. Berlin, M. Kac, Phys. Rev. **86**, 821 (1952).
12. G.S. Joyce, in *Phase Transitions and Critical Phenomena*, edited by C. Domb, M.S. Green (Academic Press, New York, 1972), Vol. 2.
13. A. Auerbach, D.P. Arovas, Phys. Rev. Lett. **61**, 617 (1988); Phys. Rev. B **38**, 326 (1988).
14. S. Sachdev, Phys. Rev. B **45**, 12377 (1992).
15. C. Timm, S.M. Girvin, P. Henelius, Phys. Rev. B **58**, 1464 (1998).
16. S. Chakravarty, B.I. Halperin, D.R. Nelson, Phys. Rev. Lett. **60**, 1057 (1988); Phys. Rev. B **39**, 2344 (1989).
17. A.V. Chubukov, S. Sachdev, J. Ye, Phys. Rev. B **49**, 11919 (1994).
18. A.V. Chubukov, O.A. Starykh, Phys. Rev. B **53**, R14729-R14732 (1996).
19. S. Ma, *Modern Theory of Critical Phenomena* (Benjamin, New York, 1973).
20. R. Abe, Prog. Theor. Phys. **48**, 1414 (1972); **49**, 113 (1973).

21. R. Abe, S. Hikami, Prog. Theor. Phys. **49**, 442 (1973); **57**, 1197 (1977).
22. Y. Okabe, M. Masutani, Phys. Lett. A **65**, 97 (1978).
23. B. Canals, D.A. Garanin, Can. J. Phys. **79**, 1323 (2001).
24. The calculations for a four sites unit cell have been done but we choose to report a two sites description for simplicity. The reader is referred to previous work if necessary [23].
25. D.A. Garanin, J. Stat. Phys. **74**, 275 (1994).
26. D.A. Garanin, V.S. Lutovinov, Solid State Commun. **50**, 219 (1984).
27. D.A. Garanin, Phys. Rev. B **53**, 11593 (1996).
28. D.A. Garanin, B. Canals, Phys. Rev. B **59**, 443 (1999).
29. D.A. Garanin, J. Stat. Phys. **83**, 907 (1996).
30. J.N. Reimers, Phys. Rev. B **46**, 193 (1992).
31. J.N. Reimers, Phys. Rev. B **45**, 7287 (1992).
32. R. Moessner, A.J. Berlinsky, Phys. Rev. Lett. **83**, 3293 (1999).
33. Authors have integrated exactly the partition function as well as the susceptibility of a tetrahedron which also corresponds in our case to the four sites unit cell of the checkerboard lattice when described as a square lattice of tetrahedra.
34. J.T. Chalker, P.C.W. Holdsworth, E.F. Shender, Phys. Rev. Lett. **68**, 855 (1992).